On a Scalable Path for Multimode SDM Transmission

Fabio A. Barbosa, *Member, IEEE,* and Filipe M. Ferreira, *Senior Member, IEEE,*

Abstract—We investigate transceiver design and digital signal processing for spatially multiplexed transmission over multimode fibers. In conventional architectures, the full spatial domain of the transmission fiber has to be detected and processed such that the modal walk-off and mixture can be estimated and equalized. These architectures scale poorly with the number of modes supported, besides the sparsity of the fiber transfer matrix is not fully exploited. Instead, here we aim to employ selective mode vector launch and detection in order to minimize the number of optical front-ends required. In this case, an ideal basis for multiplexing is offered by principal modes, that to first order are frequency independent. We show that such mode vector basis can be used for full baud rate transmission over inter-data center distances despite limited coherence bandwidth and vulnerability to environmental-induced drift of the optical channel. It is shown that crosstalk at the receiver front-end can be significantly suppressed, critically reducing the number of coherent receiver front-ends to that of spatial tributaries aimed for data transmission – as opposed to the total number of fiber modes. Residual crosstalk can still be experienced due to environmental-induced channel drift and loss of orthogonality in presence of mode dependent loss. Multiple-input single-output digital signal processing is shown to be effective in this case, with the required equalizer array size scaling sub-linearly with the number of tributaries. A multimode fiber with 156 spatial and polarization modes and optimized for low modal dispersion is considered.

Index Terms—multimode fibers, principal modes, digital signal processing, multiple-input single-output, space-division multiplexing, inter-data center.

I. Introduction

SPACE-division multiplexing (SDM) has emerged as a promising solution to overcome the capacity limit of single-mode fibers (SMFs) [1]. Amongst SDM approaches, mode multiplexing in multimode fibers (MMFs) offers the highest spatial information density and potential for integration gains at both system and component levels. However, in MMFs, co-propagating modes are affected by linear impairments such as group delay (GD) spread [2]–[7], stemming from the interplay between differential mode delay (DMD) and linear mode coupling (LMC), and mode dependent loss (MDL) [8]. The GD spreading can be compensated for using multiple-input multiple-output (MIMO) equalization [7] with computational complexity scaling with the total time spread. MMFs are then generally designed with a graded-index core in order to reduce DMD [9]. Critically, the larger the number of modes supported, the larger is the best DMD and MDL achievable [10]. To counteract the effects of MDL on transmitted signals sophisticated equalization schemes such as successive interference cancellation (SIC) can be used [11].

SDM transmission over MMF using conventional transceiver architectures requires detecting all guided modes for successful MIMO equalization of mode walk-off and mixture, otherwise system outage probability increases [12]. The number of transceiver front-ends is bounded to match the number of modes supported by the MMF, as opposed to the number of spatial tributaries required to achieve a given target throughput. In this case, large mode count fibers are not a solution to offset deployment costs because it would not be technologically feasible or economically viable to produce transceivers with as many optical front-ends as fiber modes at the system begin-of-life. To reduce MIMO equalization complexity, mode group division multiplexing (MGDM) has attracted considerable attention in a variety of combinations exploiting a subset of the total number of supported modes in MMF transmissions [13]–[15]. In the limit of MIMO-free, only two data tributaries in each mode group can be used [16] corresponding to a small fraction of the total spatial domain – note that a conventional $50\mu m$ optical fiber only has 9 mode groups but in total it supports 45 modes.

Making the number of front-ends follow the number of data tributaries would enable multimode SDM to emulate the successful evolution of wavelength-division multiplexing (WDM), i.e., to light additional channels as traffic demand grows. The SDM equivalent would be for the number of spatial data tributaries N_T transmitted over a M-mode MMF (and $M > N_T$) to be scaled progressively (e.g., doubling every 2-5 years). In this work, we propose a SDM strategy based on principal modes (PMs) that allows to significantly mitigate channel memory and modal crosstalk (XT) before the front-end of receivers and so operate with $M > N_T$. This approach offers the tantalizing prospect of exploiting MMFs and multiplexers approaching 1000 spatial and polarization modes [17], [18] to offset the deployment costs of new fibers.

PMs have firstly been investigated in [19]. The study discusses that PMs have field patterns and GDs that are independent of frequency to first order. Also, PMs were shown to form an orthogonal modal basis in the absence of MDL and the authors suggested the potential of exploring PMs to control
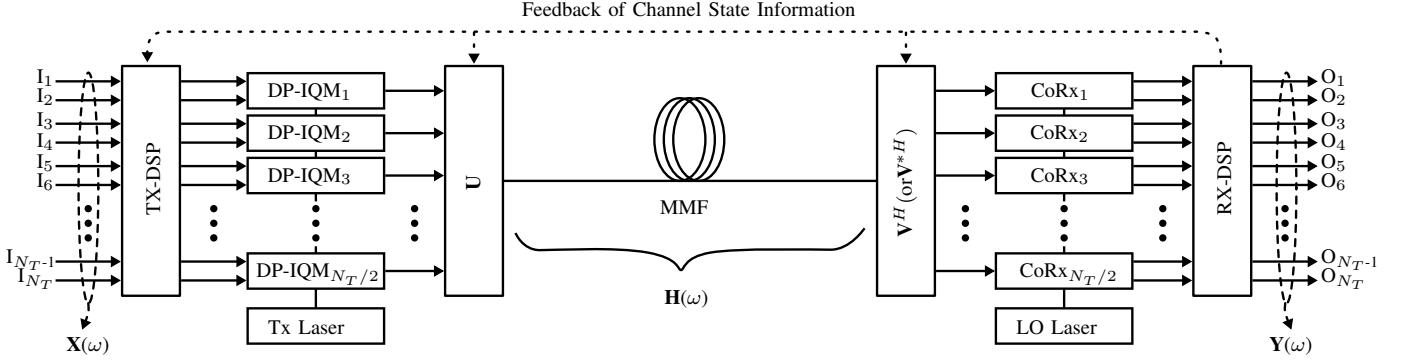
Fig. 1. Schematic diagram of the optical transmission system. Optical signals generated by $N_T/2$ dual-polarization in-phase and quadrature modulators (DP-IQMs) are spatially-multiplexed over the PMs using the mapping described by $\mathbf{U}$ and launched into a MMF with M spatial and polarization guided modes. At the receiver side, spatial tributaries are demultiplexed using $\mathbf{V}$ (or $\mathbf{V}^*$), before being detected by $N_T/2$ dual-polarization coherent receivers. CSI can be fed back from the receiver to the transmitter. I_i and O_i represent input and output data sequences, respectively.

or avoid modal dispersion in direct-detection MMF systems. Since then, studies have been conducted mostly considering the use of PMs for spatial multiplexing in the context of direct-detection [20]–[23]. In [22], the orthogonality between PMs is shown to be lost in the presence of MDL, although XT can still be partially suppressed. In [24], the frequency invariant properties of PMs has been demonstrated to be valid within a spectral range referred to as coherence bandwidth. Transmissions exceeding the coherent bandwidth of PMs lead to signals experiencing high-order modal dispersion affects, which can significantly impact PM transmissions in direct-detection systems [25]. In [26], for a 6-mode fiber and coherent single-polarization transmission, it is shown that the number of required equalizer taps is reduced for PM-based multiplexed transmissions when compared to conventional approaches – indicating a compression of channel impulse response. For a MMF with $M = 12$, in [27], we also observed reduction of channel memory and suppression of XT with PMs.

In this paper, we explore the scaling potential of PMs for coherent transmission systems with the number of optical coherent front-ends following that of data tributaries, while considering challenging channel MDL and environmentally-drift conditions. In this case, the exchange of channel state information (CSI) between the transmitter and the receiver is necessary. In [28], we conducted a numerical analysis with the calculated MMF channel to understand how XT and equalization requirements scale with the number of transmitted tributaries N_T assuming a dynamic channel. The present work extends the study in [28] where it is shown that, for slow drift ($\sim$ 1s), sufficient XT mitigation could be achieved for the channel center frequency even for $M > 100$. Here, we consider PM-based spatially multiplexed transmission over a MMF with $M = 156$ spatial and polarization modes. An in-depth description of the PM-based SDM transmission approach is presented and the results are obtained in the presence of a dynamic channel. First, an analysis assuming knowledge on the exact calculated MMF channel is conducted in order to provide insight on how XT scales with the number of transmitted tributaries. The analysis in our previous work [28] was limited to the carrier frequency, here the investigation covers the spectral occupancy of a conventional information

channel. Then, transmission simulations are conducted to investigate equalization complexity and throughput. Here, we aim at inter-data center transmission distances, where it is feasible to have feedback of CSI. Transmissions will be subject to residual XT caused by environmental-induced channel drift and loss of orthogonality in the presence of MDL as well as effects caused by limitations on the coherence bandwidth of PMs. In order to reduce the impact of such impairments on the system performance, the proposed transmission strategy includes multiple-input single-output (MISO) equalizers at the receiver. By tailoring the array size of such equalizers to the individual requirements of each PM, significant equalization complexity savings are achieved compared to the full MIMO case. We show that the combination of PMs and MISO equalizers in coherent optical system is suitable for high-speed transmission while offering a path to scaling multimode SDM transmissions.

The reminder of this paper is organized as follows. Section II discusses the fiber channel model and principal modes, including how to estimate and apply them for transmission. Section III introduces a working scheme for the allocation of the best principal modes given a specific metric and an analysis of the residual XT and interfering terms to each PM, over a 33-GHz bandwidth considering the exact calculated MMF channel that includes MDL and modal dynamics. Section IV presents and discusses the full transmission results for 33-GBaud signals. Finally, Section V provides conclusions.

II. METHODS

The optical transmission system being considered along this work is shown in Fig. 1. In the following, we discuss the channel and respective PMs as well as the proposed transmission scheme to minimize the receiver complexity.

A. Channel Model

The MMF channel in Fig. 1 can be described by a frequency-dependent $M \times M$ matrix $\mathbf{H}(\omega)$, where M is the number of supported spatial and polarization modes. It is customary to include in $\mathbf{H}(\omega)$ the impairments introduced by transceivers and other components of the transmission link. Here, for the

sake of simplicity, we consider ideal elements at both fiber ends so that $\mathbf{H}(\omega)$ captures only the MMF channel. $\mathbf{H}(\omega)$ is calculated using the multi-section approach proposed in [29], with n_{sec} fiber sections of length d_z, and a distorted core-cladding boundary. Modeling includes all main linear impairments, Rayleigh scattering loss, macro-bend loss (MBL), DMD and linear mode coupling. To investigate transmissions based on PMs over a dynamic channel, $\mathbf{H}(\omega)$ is perturbed after the round-trip time τ_{rtt} that CSI has to travel using the drift model described in [30]. The perturbations applied to $\mathbf{H}(\omega)$ are generated by random skew-Hermitian matrices whose entries are given by a complex Gaussian distribution with variance $[\sigma_{drift}(\tau_{env})]^2 = k_D/\tau_{env}$, where τ_{env} is the desired characteristic timescale of change and k_D is a scaling factor that depends on the number of modes [30]. Accordingly, the variance is increased linearly with time. The smaller τ_{env}, the larger the drift becomes, and the channel decorrelates faster with time. All n_{sec} fiber sections are considered to be dynamic and k_D is then calculated for full decorrelation of the (overall) channel matrix after a time period of τ_{env}.

B. Principal Modes for SDM Transmission

The PMs are generally different from the fiber eigenmodes. Instead, they are the eigenmodes of the so called group delay operator (GD) [31],

$$\mathbf{G}(\omega) = j\mathbf{H}^{-1}(\omega)\frac{\partial \mathbf{H}(\omega)}{\partial \omega}, \qquad (1)$$

thus, frequency independent to first order and so do not suffer from modal dispersion to first order – forming a natural basis to overcome modal dispersion [19]. Specifically, the eigenvectors and eigenvalues of $\mathbf{G}(\omega)$ correspond to the set of PMs at the fiber *input* $\mathbf{U}(\omega)$ and their GDs $\tau_1(\omega), \tau_2(\omega), \cdots, \tau_M(\omega)$, respectively. In the following, $\mathbf{U}(\omega)$ is assumed as a $M \times M$ matrix whose columns represent PMs sorted in descending order with respect to their GDs. While the set of PMs at the fiber *output* $\mathbf{V}(\omega)$ is determined by forward propagating $\mathbf{U}(\omega)$. Each PM in the input set $\mathbf{U}(\omega)$ has a corresponding PM in the output set $V(\omega)$, together forming an exclusive PM pair. Hereafter, the terms PM and PM pairs are used interchangeably. Over a certain frequency range commonly called coherence bandwidth, $\mathbf{H}(\omega)$ can be satisfactorily approximated by

$$\mathbf{H}(\omega) \approx \mathbf{V}(\omega_0)\mathbf{\Lambda}(\omega)\mathbf{U}(\omega_0)^H \qquad (2)$$

where ω_0 represents channel central frequency and $\mathbf{\Lambda}(\omega) = \text{diag}\{e^{j(\omega-\omega_0)\tau_1(\omega_0)}, \cdots, e^{j(\omega-\omega_0)\tau_M(\omega_0)}\}$. Note that, the central frequency ω_0 will be dropped when referring to the PMs and their GDs hereafter. PMs form an orthogonal multiplexing basis at both fiber ends. However, in the presence of MDL such orthogonality is partially lost. Nevertheless, crosstalk can still be partially suppressed by multiplexing over the PMs, as will be shown in Sec. III. The coherence bandwidth over which PMs can be assumed frequency independent is application specific [25]. In extreme cases, coherence bandwidths of several THz have been shown for a wide range of M-modes over lengths shorter than 1 km [32]. In this work, and for the fiber considered, PMs have a range of coherence bandwidths that in many cases approaches the spectral width of the transmission channel.

As depicted in Fig. 1, the assumption in this work is that CSI can be fed back from the receiver to the transmitter such that the SDM system can take full advantage of the PMs, except for channel drift being considered. This is, the set of PM pairs $\mathbf{U}_{(t=t_0)}$ and $\mathbf{V}_{(t=t_0)}$ obtained at a time $t = t_0$ is applied for SDM transmission, after the round trip time from receiver to transmitter τ_{rtt}, over the drift-perturbed channel $\mathbf{H}_{drifted}(\omega) = \mathbf{H}(\omega, t = t_0+\tau_{rtt})|_{\sigma_{drift}(\tau_{env})}$. With this approach, the residual channel at the input of the receiver becomes

$$\mathbf{H}_{res}(\omega) = \mathbf{\Lambda}_{(t=t_0)}^{-1}(\omega)\mathbf{V}_{(t=t_0)}^H\mathbf{H}_{drifted}(\omega)\mathbf{U}_{(t=t_0)} \qquad (3)$$

where $(\cdot)^H$ is the Hermitian operator. The residual channel $\mathbf{H}_{res}(\omega)$ in (3) captures the residual XT induced by channel drift and MDL. Considering the channel drift over time is critical to understanding the potential of using PMs for SDM, since the set of PMs may not be fully valid for the (perturbed) channel after τ_{rtt}.

Modal multiplexing at the transmitter and demultiplexing at the receiver are performed, respectively, following $\mathbf{U}$ and $\mathbf{V}$. These matrices represent mapping from signals to input and output PMs in terms of the local ideal fiber modes. Here lies one of the critical advantages of using PMs: *being frequency independent to first order, the mapping between signals and PMs can be implemented in the optical domain via one matrix operation.* For such operation, one could utilize programmable mode (de)multiplexers that are realized by combining spatial light modulators (SLMs) and multi-plane light conversion (MPLC) [33]–[35]. Another option is to use photonic integrated chips (PICs), e.g., with a mesh of Mach-Zehnder interferometers (MZIs) in a feed-forward arrangement [36]–[38]. By applying the mappings described by $\mathbf{U}$ and $\mathbf{V}$ in the optical domain (as opposed to in the electrical domain), the channel memory and the accumulated of mode coupling are reduced at the receiver front-end, potentially reducing to N_T (or $N_T/2$ for dual polarization receivers) the number of optical front-ends necessary to transmit and detect N_T spatial tributaries, importantly, where $N_T < M$.

Here, our objective is to assess the capability of the proposed PM-based approach to reduce the accumulated modal crosstalk at the receiver front-end for a full baud rate data channel, extending our previous results [28] obtained looking just at the carrier frequency. In this case, the transmission signals bandwidth compare to that of the coherence bandwidth of PMs, leading to increased residual XT and high-order modal dispersion effects can became significant. Eventually, equalization is necessary to mitigate these impairments. As will be shown in sections Sec. III and IV, for each PM, residual XT is limited to a small set of interfering neighbors. Then, taking advantage of this, we consider MISO equalization tailored to individual PM requirements so as to achieve computational complexity that is a fraction of that of full MIMO in the conventional architecture.

C. Channel and Principal Modes Estimation

Estimation of the $M \times M$ channel $\mathbf{H}(\omega)$ can be performed by inserting periodical training sequences (TSs) into the data transmitted in each tributary. Mutually orthogonal TSs are

preferred when training overhead is to be minimized. In this work, the L-length TS transmitted on the p-th tributary is given by the inverse discrete Fourier transform (IDFT) of a frequency-domain sequence defined as

$$S_p[k] = \begin{cases} C[k], & k = p + lM \\ 0, & otherwise, \end{cases} \quad (4)$$

where $C[k]$ is a binary phase shift keying (BPSK) sequence, k is the discrete frequency index, and $l = [0, 1, \cdots, \lfloor L/M - 1 \rfloor]$. From (4), it follows that each tributary uses a different set of discrete frequencies for training. At the receiver, a least-square (LS) frequency domain channel estimation is performed. The channel between the j-th *transmitter* and the i-th *receiver*, i.e. $\hat{H}_{i,j}[k]$, is estimated as

$$\hat{H}_{i,j}[k] = \frac{R_i[k]}{S_j[k]}, \quad k = j + lN, \quad (5)$$

where $R_i[k]$ is the TS received at the i-th receiver. An additional interpolation and extrapolation step is required to estimate the channel over all frequency positions. Furthermore, one can apply to the estimates a smoothing filter in order to reduce artifacts. For orthogonal frequency division multiplexing (OFDM) transmissions, a similar approach can be applied. An alternative method is to employ constant amplitude zero auto-correlation (CAZAC) sequences combined with LS time domain channel estimation [39, Sec. 3], before calculating a discrete Fourier transform (DFT) to obtain an estimate of $\mathbf{H}(\omega)$.

To calculate the sets of PMs, the GD operator in (1) needs to be computed with channel estimates $\hat{\mathbf{H}}(\omega)$ using a finite difference approximation to the derivative. Alternatively, one can resort to approximating the GD operator as done in [32], for channel estimates generated via off-axis digital holograph, by $\mathbf{G}(\omega_c) \approx j1/(\omega_+ - \omega_-)\mathbf{H}(\omega_-)\mathbf{H}^{-1}(\omega_+)$, where ω_- and ω_+ represent frequencies to either side of a central value ω_c. Both methods require adjustment of the frequency spacing. A small spacing can lead to calculations being affected by artifacts of channel estimates, while the opposite may generate an improper approximation to the differentiation. Recently, an alternative method has been proposed for PM estimation that is referred to mode-dependent signal delay method [40]. This method allows to estimate the GD operator through measurements of group delays of various combinations of modes launched into a MMF. In [41], the estimation framework was extended to consider receiver noise and MDL.

In this work, we also modify the set of output PMs so that the residual channel, at the carrier frequency (ω_0), is perfectly diagonalized. A similar approach has been shown in [22]. The zero-forcing equalizer

$$\mathbf{W}_{res}(\omega = \omega_0, t = t_0) = \left(\mathbf{V}_{(t=t_0)}^H \mathbf{H}(\omega = \omega_0, t = t_0)\mathbf{U}_{(t=t_0)}\right)^\dagger, \quad (6)$$

where $(\cdot)^\dagger$ is the pseudo-inverse function, is applied to the output PMs such that

$$\mathbf{V}_{(t=t_0)}^* = \left(\mathbf{V}_{(t=t_0)}\mathbf{W}_{res}^H(\omega = \omega_0, t = t_0)\right)^H. \quad (7)$$

The new set of PMs (including both input $\mathbf{U}$ and output PMs $\mathbf{V}^*$) is indicated hereafter by PMs*. Note that operations described in (6) and (7) are only performed at instant $t = t_0$.

For the rest of this paper, we drop the superscript $(\cdot)_{(t=t_0)}$ from matrices $\mathbf{U}$, $\mathbf{V}$ and $\mathbf{V}^*$, since PMs are always derived for a given channel realization $\mathbf{H}(\omega = \omega_0, t = t_0)$ and used for transmission over a drifted channel $\mathbf{H}_{drifted}(\omega)$.

III. SCALING OF GDs AND XT FOR TRANSMISSIONS EXPLOITING PMs

This section investigates numerically the use of PM pairs for the transmission of N_T tributaries and N_T optical front-ends over a MMF with $M = 156$ spatial and polarization modes. An inter-data center scenario consisting of a 10-km fiber link is considered. The fiber is modeled assuming 100 fiber sections of 100 m. All impairments are calculated for a graded-core trench-assisted fiber optimized for a refractive index contrast of $\Delta n_{co} = 0.01$ and a 30 μm radius following [42]. Mode coupling is modeled considering a distorted core-cladding boundary for a radial displacement of $0.3 \mu m$ – an accumulated crosstalk of approximately -13 dB is observed after 10 km. The MBL corresponding to one 60 mm radius loop is applied every section, leading to some of the modes in the last mode group to be severely attenuated so that the total number of useful modes is 144. The Rayleigh scattering loss ranges from 0.197 dB/km for LP_{01} to 0.173 dB/km for the LP mode of the highest order.

The analysis of the PMs is conducted in this section considering the exact calculated MMF channel $\mathbf{H}(\omega)$ as well as the residual channel $\mathbf{H}_{res}(\omega)$ in (3) for several τ_{env} values. Reflecting typical acquisition time of channel transfer functions using digital holography ($\sim 0.1 - 100$s) as well as the long term stability of PMs reported in [32], τ_{env} is considered ranging from 0.01s to 10s.[1] The aim is to provide insights on how XT scales with the number of PM pairs selected for transmission, considering a channel bandwidth of 33 GHz (see Sec. IV for full data transmission). Fig. 2(a) shows a typical $\mathbf{H}(\omega = \omega_0)$ (at 193.41 THz) while Figs. 2(b) and 2(c) show the end-to-end residual channel when using all PM pairs ($\mathbf{U}$ and $\mathbf{V}$) calculated for $\mathbf{H}(\omega = \omega_0, t = t_0)$ to transmit over $\mathbf{H}_{drifted}(\omega) = H(\omega, t = t_0 + \tau_{rtt})|_{\sigma_{drift}(\tau_{env})}$, with $\tau_{env} = 10$s and $\tau_{env} = 1$s, respectively. Off-diagonal terms with reduced power in Figs. 2(b) and 2(c), dubbed here as interfering terms, are mostly caused by the mismatch between the PMs used and the drifted channel $\mathbf{H}_{drifted}(\omega)$. In fact, the number and power of these terms increase with drift strength, as can be observed comparing Figs. 2(b) and 2(c). For $\tau_{env} = \infty$, i.e. static channel, it was verified that interfering terms were negligible, except for a small fraction of N_T-PM pairs ($\approx 1\%$) whose orthogonality was affected by MDL. Smaller τ_{env} values are considered in the following.

A. Strategy to Select Groups of PMs for Transmission

It is assumed that the number of data tributaries required will increase progressively during the system lifetime. Thus, a

---

[1]A range of studies for SMF cables has shown that state of polarization can oscillate as fast as 50Hz for aerial cables [43], [44], or remain constant as long as 20min in buried cables [45] with isolated fast changes [46]. However, for MMF cables, characterization data on channel dynamics is still an ongoing research topic.
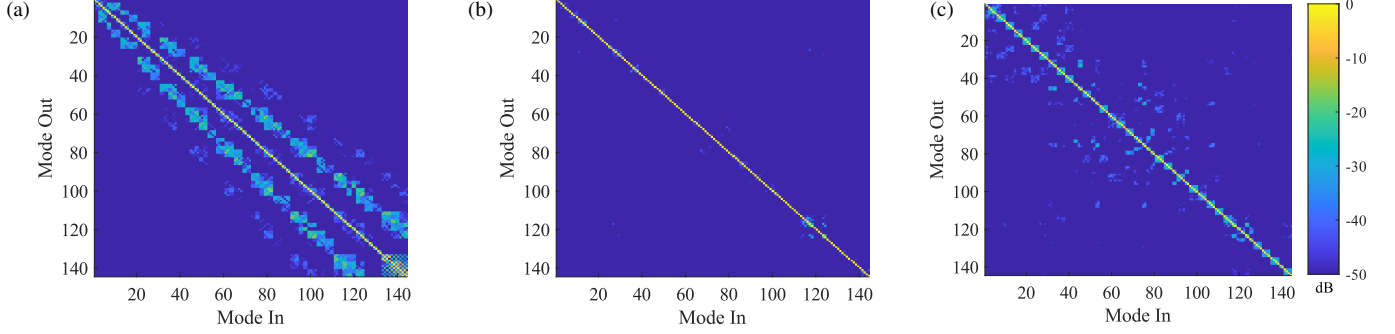
Fig. 2. Typical (a) MMF channel transfer matrix $\mathbf{H}(\omega = \omega_0)$ at 193.41 THz. Residual channel transfer matrix, $(\mathbf{V}^{\mathrm{H}})_{t=t_0}\mathbf{H}_{drifted}(\omega = \omega_0)\mathbf{U}_{t=t_0}$, for (b) $\tau_{env} = 10$s and (c) $\tau_{env} = 0.1$s. The results consists on analysis of the 10-km MMF with $M = 156$ spatial and polarization modes. The channel is modeled according to [29] with 100 fiber sections of 100m for a distorted core-cladding boundary (of 1% of the core radius). Note that, due to MBL, 12 modes belonging to the last mode group are severely attenuated and are not shown in this figure. PMs are calculated through the eigenvalue decomposition of $\mathbf{G}(\omega)$.
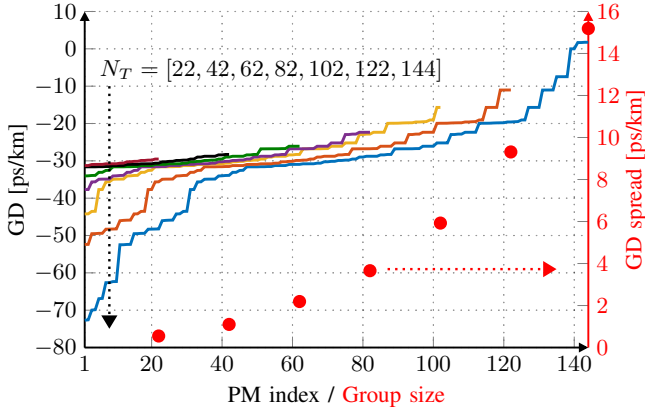

Fig. 3. GD and GD spread as a function of PM index and group size, respectively, for each group of size $N_T = [22, 42, 62, 82, 102, 122, 144]$. Groups are formed by selecting the PMs according to their deviation from the GD median, from the lowest onwards. *Note that is this case, the x-axis is relative to each group of N_T PM pairs.*

strategy to select a group of N_T PM pairs $(N_T < M)$ for the transmission of N_T tributaries is required. In this work, we simply select PM pairs by their GD deviation from the median value given all GDs, from the lowest deviation onwards. This is done in order to minimize any unwanted channel impulse response spread and so reduce equalization complexity shall MIMO be required to untangle some of the data tributaries. Fig. 3 shows the outcome of such selection. *Our strategy allows to increase, with the granularity of one, the number of spatial tributaries.* In this work we concentrate the analysis for the arbitrary cases where the number of tributaries is varied for $N_T = [22, 42, 62, 82, 102, 122, 144]$. The GDs are presented in ascending order for the individual PM pairs that composes each group of size N_T (lines and right y-axis). The vertical dotted arrow indicates the direction of increasing N_T. The GD spread within each group is also shown (markers and left y-axis). All values were calculated using the channel $\mathbf{H}(\omega)$.

B. Results and Discussions

We conducted analysis of $\mathbf{H}_{res}(\omega)$ considering groups of N_T PM pairs for transmission and N_T transceiver front-ends for detection – group selection followed the GDs indicated in Fig. 3. Note that, transmission and detection using a group

of N_T PM pairs translates into selecting specific columns of $\mathbf{U}$ and $\mathbf{V}$ (or $\mathbf{V}^*$), respectively. Firstly, we assess the XT per PM that is obtained when all PMs of each group are used for simultaneous transmission. For a given frequency position and channel of interest, XT is assumed to be the sum of the power of all interfering terms present on the residual channel matrix $\mathbf{H}_{res}(\omega)$ (e.g, off-diagonal terms visible in Fig. 2(b)) divided by the power of the respective spatial channel (diagonal term). Calculations are performed at frequencies spaced by 0.5 GHz covering an interval of 33 GHz centered at 193.41 THz. Fig. 4(a) presents the XT per PM averaged over such frequency interval when $\tau_{env} = 1$s. For the sake of simplicity, data points are presented in ascending order for each N_T. Dashed and solid lines indicate the results obtained with the (original) set of PMs and the set that includes $\mathbf{V}^*$ given by Eq. (7) (PMs*), respectively. The XT experienced by each PM is the outcome of contributions originating at environmental-induced channel drift and at loss of orthogonality in presence of MDL. The overall level of XT within the groups increases with N_T as a result of the increase in the number of interfering terms with the group size. It can also be observed that the processing described in (7) offers small gain in terms of XT suppression over such channel conditions. Further investigations have shown that, even for the central frequency ($\omega = \omega_0$) only, the advantages of its usage for the dynamic channel is present mostly for large groups (e.g., with $N_T > 82$). However, in Sec. IV we show that when PMs are computed using channel estimates, the operation described in (7) contributes to higher performance in most cases. For the remaining of this section, the analysis is restricted to the set of PMs*.

Fig. 4(b) shows, in ascending order, the XT averaged over the 33-GHz bandwidth for $N_T = 144$ and for $\tau_{env} = [10, 1, 0.1, 0.02, 0.01]$s. The vertical dotted arrow indicates the direction of decreasing τ_{env}. The capability of XT suppression with PMs is reduced as the channel starts to drift faster (i.e., as τ_{env} reduces). This is caused because the set of PMs may not be fully valid for the (perturbed) channel.

In order to gain more insight into the XT experienced by the PMs, we also investigated the number of interfering terms to each PM transmitted in a group of size N_T. For this analysis, the weaker interfering terms are neglected. This is done by
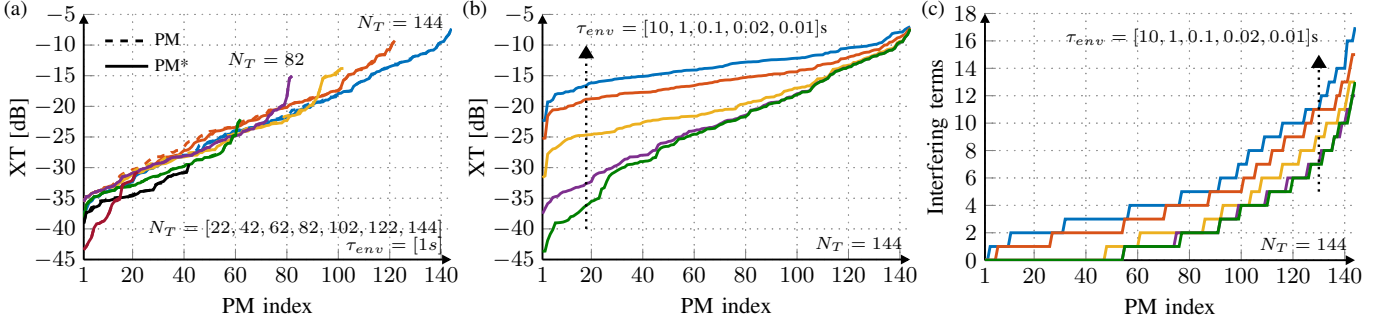
Fig. 4. Investigating $\mathbf{H}_{res}(\omega)$, average XT over a bandwidth of 33 GHz (a) assuming $\tau_{env} = 1$s and the groups of size N_T from Fig. 3 and (b) for $N_T = 144$ and $\tau_{env} = [10, 1, 0.1, 0.02, 0.01]$s. Dashed lines correspond to sets of PMs, while solid lines to sets of PMs including processing specified in (7). Results are sorted in ascending order. (c) Number of interfering terms, evaluated over the 33-GHz-bandwidth for $N_T = 144$. The smallest group of interfering terms that amounts to a XT ≤ -20 dB is neglected. Results are sorted following the same order of Fig. 4(b).

neglecting the smallest group of interfering terms that amounts to a XT level below a certain threshold. In practical terms, this means that the contribution of the neglected terms to the overall XT of a given PM would not be compensated, but assumed as noise that affects the signal-to-noise ratio (SNR). Here, the threshold is set to XT ≤ -20 dB. Thus, an SNR of 20 dB is achievable should the channel additive noise allows and equalization is capable of mitigating the XT contribution from the remaining interfering terms. Fig. 4(c) shows the results for a group of $N_T = 144$ PM pairs and $\tau_{env} = [10, 1, 0.1, 0.02, 0.01]$s following the same PM indexing in Fig. 4(b). Analyzing Figs. 4(b) and 4(c) jointly, one can observe that XT increases because the number of interfering terms to each PM grows with decreasing τ_{env}. However, the number of interfering terms to a given PM does not increase significantly with the strength of the channel drift, especially comparing with the XT increase in Fig. 4(b). This indicates that it is the strength of interferes that mostly contributes to the increase of XT with the drift as opposed to an increase in the number of the interferes. In addition, the wide range in the number of interfering terms in Fig. 4(c) suggests that PMs can have very distinct equalization requirements – with many PMs requiring just single-input single-output (SISO) or low-order multiple-input single-output (MISO) equalization. Sec. IV provides an analysis on array size requirements for MISO equalizers.

IV. TRANSMISSION SIMULATIONS

In this section, transmission simulations are performed considering the same fiber channel described in Sec. III. The transmitted tributaries consist on 33-GBd 16-QAM signals with TSs of length $L = 8192$ symbols appended to the beginning of the payload. The TSs are generated as shown in Sec. II. An initial transmission of 144 tributaries is performed in order to generate $\hat{\mathbf{H}}(\omega)$ using the TSs and LS frequency domain channel estimation. Then, the PMs at fiber input and output are estimated based on $\hat{\mathbf{H}}(\omega)$ and used for transmission over the drift-perturbed channel $\mathbf{H}_{drifted}(\omega)$, with $\tau_{env} = [10, 1, 0.1, 0.02, 0.01]$s. Investigations are conducted with groups of $N_T = [22, 42, 62, 82, 102, 122, 144]$ data tributaries. They are transmitted implementing the mappings described by $\mathbf{U}$ and $\mathbf{V}$ (or $\mathbf{V}^*$) according to the PMs that are

selected following the same strategy discussed in the previous section. At the transmitter, tributaries are optically multiplexed prior to launching into the MMF using $\mathbf{U}$. At the receiver, tributaries are optically demultiplexed with $\mathbf{V}$ (or $\mathbf{V}^*$). Ideal transceivers as well as optical devices for mapping between signals and PMs are considered. It is important to stress that the number of optical front-ends employed for transmission and detection matches the number of data tributaries N_T.

The optical signal-to-noise ratio (OSNR) is controlled and set to 35 dB independently of the number of tributaries transmitted by adding amplified spontaneous emission (ASE) noise as additive white Gaussian noise (AWGN) to the signals. No impairments are considered other than ASE noise and fiber-related effects (see Sec. IIB and III for the full list of parameters). At the receiver, the estimated residual channel is employed to perform minimum mean square error (MMSE) MISO equalization. The equalizers are implemented in the frequency domain utilizing an overlap-save approach with a 8192-point fast Fourier transform (FFT) and an overlap of 1024 samples. We opt for MISO equalizers due to the unequal equalization requirements of each PM suggested by the analysis conducted in the previous section (see Fig. 4(c)). The MISO equalizer array size is varied from 1 (SISO case) to N_T. This allows understanding the contribution of the interfering terms to the performance of a given PM and determining how performance scales with equalization complexity. The array size is increased by adding the terms with highest contribution to the XT experienced by the PM under analysis.

The SNR of received constellations is then evaluated for the different configurations of N_T, τ_{env} and MISO array size. The SNR of the constellation received at the i-th tributary is $\text{SNR}_i = \text{E}\{|\mathbf{x}_i|^2\}/\text{E}\{|\mathbf{y}_i - \mathbf{x}_i|^2\}$, where $\mathbf{x}_i$ and $\mathbf{y}_i$ are the transmitted and received symbols, respectively. Subsequently, the SNR values are used to estimate the total throughput for a bandwidth B and a given number of spatially-multiplexed tributaries N_T as

$$\text{Throughput} = B \sum_{i}^{N_T} \log_2(1 + \text{SNR}_i). \tag{8}$$

In order to use this expression, we assume that SNR performance remains same for higher-cardinality constellations as well as for any number of WDM channels in B.

A. Results and Discussions

Fig. 5 shownns the average SNR of received constellations versus the MISO array size for $\tau_{env} = 0.1$s and $N_T = [82, 144]$. Solid and dashed lines illustrate the results obtained with V^* and V, respectively. Better average performance is obtained when using V^* for demultiplexing, similarly to what was shown in [22]. This results differs from Sec. III, where with exact knowledge of the MMF channel, using V^* did not produce significant gains. Here we conjecture that the approach described in (7) produces better PM approximations in the presence of channel estimate artifacts. Hereafter, the results are restricted to the set of PMs that includes V^* for demultiplexing.

Fig. 6 presents the required MISO array size for each PM to achieve a target SNR ≥ 24 dB for $\tau_{env} = [1, 0.1, 0.01]$s and $N_T = [82, 144]$. For the sake of clarity, the results are shown in ascending order. The MISO array size increases as τ_{env} decreases, but the outcomes confirm that different PM pairs have distinct equalization requirements. In fact, some of the PM pairs achieve SNRs above 27 dB for MISO array sizes around 6, even for $\tau_{env} = 0.01$s and both N_T values. Despite the vulnerability to environmental-induced drift of the optical fiber channel, the results indicate that PMs can be used for coherent transmission yet leading to reduction of equalization complexity compared to the $N_T \times N_T$ MIMO case.

The analysis of total throughput is shown in Fig. 7 for $\tau_{env} = 0.1$s and different values of N_T. We consider that PMs are used for SDM transmission occupying a spectral bandwidth of 5 THz over the C-band. Note that WDM transmissions require the system shown in Fig. 1 to be replicated to each wavelength (i.e, 151-times $\approx$ 5THz/33GHz). Multimode WDM multiplexers and demultiplexers should then be added after and before the spatial multiplexers, respectively. In Fig. 7, the throughput is shown for each N_T as a function of the normalized MISO complexity. The latter is given by the sum of the MISO array size of each PM_i (MISO_i) divided by that of the full MIMO case, i.e., $1/(M^2) \sum_i^{N_T} \text{MISO}_i$. Each line starts from the SISO case. Interestingly, the last point differs from the $N_T \times N_T$ MIMO. This is because the performance of some individual PM pairs reach SNR plateaus and, for these, the MISO array size used is the shortest one required to be within 0.1 dB of the SNR plateau. Importantly, from Fig. 7, one can increase throughput by addressing more modes while *keeping to the same total equalization complexity*. Here, for example, with an equalization complexity approximately $100\times$ smaller than that of the $N_T \times N_T$ MIMO scenario, by increasing the number of addressed modes from 22 to 102, it is possible to transmit from roughly 1 to 3.6 Pb/s. Furthermore, in Fig. 7, it can be seen that for small group sizes, $N_T < 42$, throughput can be near-maximum with near-SISO complexity. Finally, the results in Fig. 7 indicate that for a given target throughput, 3 to 4 Pb/s, one can operate either with fewer PMs at higher complexity or more PMs at lower complexity – opening interesting challenges for system design. This system architecture allows trading larger array integration sizes for savings in equalization complexity for a given target throughput.

In summary, the results in Fig. 6 and Fig. 7 show that the proposed PM-based SDM system allows progressively
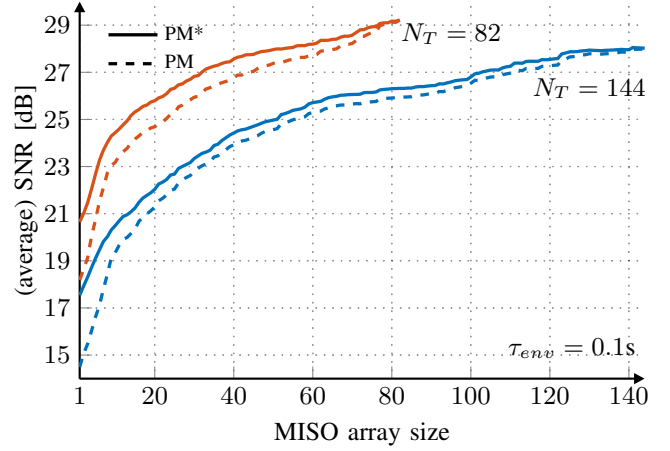

Fig. 5. Average SNR of received constellations versus MISO array size for $\tau_{env} = 0.1$s and $N_T = [82, 144]$. The results obtained with the set of PMs* (including processing described in (7)) and PMs are indicated by the solid and dashed lines, respectively.
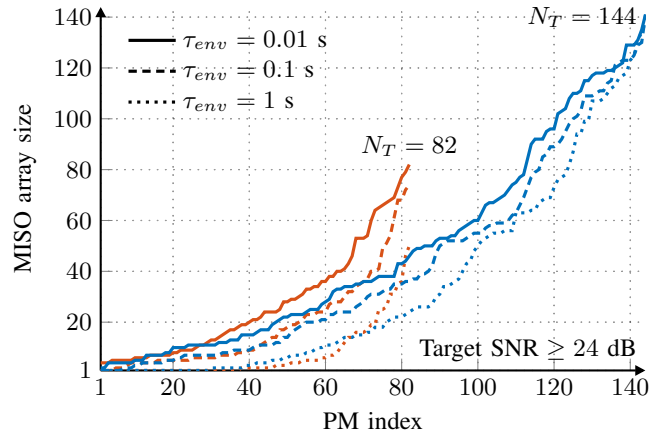

Fig. 6. Required MISO array size for each PM to achieve a target SNR ≥ 24 dB for $\tau_{env} = [1, 0.1, 0.01]$s and $N_T = [82, 144]$. Arbitrary PM indexing is used such that MISO array size is in ascending order.

increasing the number of spatial tributaries N_T, while keeping to N_T coherent transceiver front-ends and with MISO array size significantly smaller than N_T.

V. CONCLUSION

Conventional SDM architectures require detecting and processing the full spatial domain in MMFs such that the walk-off and mode mixing can be estimated and equalized. These architectures scale poorly with the number of guided modes preventing the deployment of large mode count fibers. Critically, in this work, through selective mode vector generation and detection, and modified principal modes, we show that the number of transceiver front-ends can be made to match that of data tributaries. We investigated data transmission over the principal modes of a MMF with $M = 156$ spatial and polarization modes while considering a dynamic channel. We showed that, by mapping data tributaries to principal modes, in the optical domain, XT can be suppressed at the front-end of coherent receivers. Any residual XT, due to channel drift, MDL and/or channel estimation errors, is then compensated
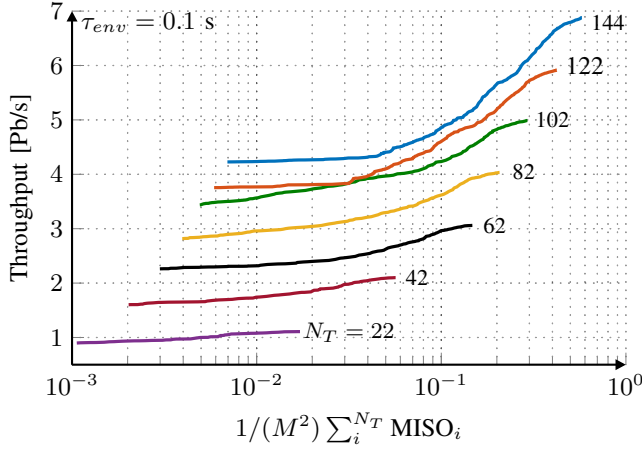
Fig. 7. Throughput versus the sum of MISO array sizes of each PM normalized by the full MIMO case. The results consider that PMs are used for SDM transmission over a spectral bandwidth of 5 THz in the C-band. The throughput is computed using (8) for $\tau_{env} = 0.1$s and $N_T = [22, 42, 62, 82, 102, 122, 144]$.

for using low-order MISO equalizers. A throughput analysis showed that principal modes can be used to perform high-speed data transmission for inter-data center distances with equalization complexity scaling sub-linearly with the number of data tributaries. The results show that it is possible to transmit up to 4 Pb/s over the C-band when allowing for an equalization complexity $\approx 100\times$ smaller than that of the full MIMO case. Following this study, we will be considering MMFs with larger mode count, for which even larger throughput is expected. Finally, the proposed channel diagonalization scheme opens a scalable path to increase throughput in SDM transmission systems while keeping equalization complexity following that of parallel single-mode transmission systems.

ACKNOWLEDGMENTS

REFERENCES

[1] D. J. Richardson, J. M. Fini, and L. E. Nelson, "Space-division multiplexing in optical fibres," *Nature Photonics*, vol. 7, no. 5, pp. 354–362, apr 2013.

[2] F. Ferreira, P. Monteiro, and H. Silva, "Semi-analytical model for linear modal coupling in few-mode fiber transmission," in *2012 14th International Conference on Transparent Optical Networks (ICTON)*, 2012, pp. 1–4.

[3] A. Mecozzi, C. Antonelli, and M. Shtaif, "Intensity impulse response of SDM links," *Opt. Express*, vol. 23, no. 5, pp. 5738–5743, Mar 2015. [Online]. Available: http://opg.optica.org/oe/abstract.cfm?URI=oe-23-5-5738

[4] C. Antonelli, A. Mecozzi, and M. Shtaif, "The delay spread in fibers for SDM transmission: dependence on fiber parameters and perturbations," *Opt. Express*, vol. 23, no. 3, pp. 2196–2202, Feb 2015. [Online]. Available: http://opg.optica.org/oe/abstract.cfm?URI=oe-23-3-2196

[5] F. M. Ferreira, C. S. Costa, S. Sygletos, and A. D. Ellis, "Semi-analytical modelling of linear mode coupling in few-mode fibers," *Journal of Lightwave Technology*, vol. 35, no. 18, pp. 4011–4022, 2017.

[6] J. Vuong, P. Ramantanis, A. Seck, D. Bendimerad, and Y. Frignac, "Understanding discrete linear mode coupling in few-mode fiber transmission systems," in *2011 37th European Conference and Exhibition on Optical Communication*, 2011, pp. 1–3.

[7] B. Inan, B. Spinnler, F. Ferreira, D. van den Borne, A. Lobato, S. Adhikari, V. A. J. M. Sleiffer, M. Kuschnerov, N. Hanik, and S. L. Jansen, "DSP complexity of mode-division multiplexed receivers," *Opt. Express*, vol. 20, no. 10, pp. 10859–10869, May 2012. [Online]. Available: http://opg.optica.org/oe/abstract.cfm?URI=oe-20-10-10859

[8] A. Lobato, F. Ferreira, M. Kuschnerov, D. van den Borne, S. L. Jansen, A. Napoli, B. Spinnler, and B. Lankl, "Impact of mode coupling on the mode-dependent loss tolerance in few-mode fiber transmission," *Opt. Express*, vol. 20, no. 28, pp. 29776–29783, Dec 2012. [Online]. Available: http://opg.optica.org/oe/abstract.cfm?URI=oe-20-28-29776

[9] F. M. Ferreira, D. Fonseca, and H. J. A. da Silva, "Design of few-mode fibers with m-modes and low differential mode delay," *Journal of Lightwave Technology*, vol. 32, no. 3, pp. 353–360, 2014.

[10] P. Sillard, D. Molin, M. Bigot-Astruc, K. de Jongh, and F. Achten, "Rescaled multimode fibers for mode-division multiplexing," *J. Lightwave Technol.*, vol. 35, no. 8, pp. 1444–1449, Apr 2017.

[11] E. S. Chou and J. M. Kahn, "Successive interference cancellation on frequency-selective channels with mode-dependent gain," *Journal of Lightwave Technology*, vol. 40, no. 12, pp. 3729–3738, 2022.

[12] P. J. Winzer and G. J. Foschini, "MIMO capacities and outage probabilities in spatially multiplexed optical transport systems," *Opt. Express*, vol. 19, no. 17, pp. 16680–16696, Aug 2011. [Online]. Available: http://opg.optica.org/oe/abstract.cfm?URI=oe-19-17-16680

[13] P. Boffi, N. Sambo, P. Martelli, P. Parolari, A. Gatto, F. Cugini, and P. Castoldi, "Mode-group division multiplexing: Transmission, node architecture, and provisioning," *Journal of Lightwave Technology*, vol. 40, no. 8, pp. 2378–2389, 2022.

[14] A. Gatto, P. Parolari, R. S. Luís, G. Rademacher, B. J. Puttnam, R. Emmerich, C. Schubert, G. Ferri, F. Achten, P. Sillard, P. Martelli, G. D. Sciullo, F. Graziosi, A. Marotta, A. Mecozzi, C. Antonelli, and P. Boffi, "Partial MIMO-based mode division multiplexing transmission over the first field-deployed 15-mode fiber in metro scenario," in *Optical Fiber Communication Conference (OFC) 2023*, 2023, p. M2B.3.

[15] L. Dallachiesa, R. Ryf, N. K. Fontaine, M. Mazur, H. Chen, P. Sillard, G. Ferri, F. Achten, A. Carena, A. Nespola, A. Marotta, A. Mecozzi, and C. Antonelli, "Mode-group-division multiplexing over a deployed 15-mode-fiber cable," in *Optical Fiber Communication Conference (OFC) 2023*, 2023, p. M2B.4.

[16] A. Gatto, P. Martelli, P. Parolari, N. Sambo, P. Castoldi, and P. Boffi, "Mode group division multiplexing in 5 mode-group fmf enabling MIMO-free solutions," *IEEE Photonics Technology Letters*, vol. 34, no. 21, pp. 1167–1170, 2022.

[17] F. M. Ferreira and F. A. Barbosa, "Towards 1000-mode optical fibres," 2022. [Online]. Available: https://arxiv.org/abs/2206.09855

[18] N. K. Fontaine, H. Chen, M. Mazur, L. Dallachiesa, K. Kim, R. Ryf, D. Neilson, and J. Carpenter, "Hermite-gaussian mode multiplexer supporting 1035 modes," in *Optical Fiber Communication Conference (OFC) 2021*. Optica Publishing Group, 2021, p. M3D.4.

[19] S. Fan and J. M. Kahn, "Principal modes in multimode waveguides," *Opt. Lett.*, vol. 30, no. 2, pp. 135–137, Jan 2005.

[20] X. Shen, J. M. Kahn, and M. A. Horowitz, "Compensation for multimode fiber dispersion by adaptive optics," *Opt. Lett.*, vol. 30, no. 22, pp. 2985–2987, Nov 2005.

[21] R. A. Panicker, A. P. T. Lau, J. P. Wilde, and J. M. Kahn, "Experimental comparison of adaptive optics algorithms in 10-gb/s multimode fiber systems," *Journal of Lightwave Technology*, vol. 27, no. 24, pp. 5783–5789, 2009.

[22] A. A. Juarez, C. A. Bunge, S. Warm, and K. Petermann, "Perspectives of principal mode transmission in mode-division-multiplex operation," *Opt. Express*, vol. 20, no. 13, pp. 13810–13824, Jun 2012.

[23] A. Vijay and J. M. Kahn, "Effect of higher-order modal dispersion in direct-detection mode-division-multiplexed links," *Journal of Lightwave Technology*, vol. 41, no. 6, pp. 1670–1683, 2023.

[24] M. B. Shemirani, W. Mao, R. A. Panicker, and J. M. Kahn, "Principal modes in graded-index multimode fiber in presence of spatial- and polarization-mode coupling," *Journal of Lightwave Technology*, vol. 27, no. 10, pp. 1248–1261, 2009.

[25] K.-P. Ho and J. M. Kahn, "Mode coupling and its impact on spatially multiplexed systems," in *Optical Fiber Telecommunications Volume VIB*, I. Kaminow, T. Li, and A. Willner, Eds. Amsterdam, NL: Elsevier, 2013, pp. 491–568.

[26] A. Juarez, D. Kroushkov, S. Warm, C. A. Bunge, and K. Petermann, "Comparison of MIMO receiver complexity in a mdm transmission system using principal modes and LP-modes as carriers," in *2013 ITG Symposium Proceedings - Photonic Networks*, 2013, pp. 1–4.

[27] F. A. Barbosa and F. M. Ferreira, "Scaling spatial multiplexing with principal modes," in *2022 IEEE Photonics Conference (IPC)*, 2022, pp. 1–2.

[28] ——, "On the advantages of principal modes for multimode SDM transmission systems," in *Optical Fiber Communication Conference (OFC) 2023*, 2023, p. Th2A.31.

[29] F. M. Ferreira, C. S. Costa, S. Sygletos, and A. D. Ellis, "Semi-analytical modelling of linear mode coupling in few-mode fibers," *Journal of Lightwave Technology*, vol. 35, no. 18, pp. 4011–4022, 2017.

[30] K. Choutagunta, I. Roberts, and J. M. Kahn, "Efficient quantification and simulation of modal dynamics in multimode fiber links," *Journal of Lightwave Technology*, vol. 37, no. 8, pp. 1813–1825, 2019.

[31] D. Askarov and J. M. Kahn, "Long-period fiber gratings for mode coupling in mode-division-multiplexing systems," *J. Lightwave Technol.*, vol. 33, no. 19, pp. 4032–4038, Oct 2015. [Online]. Available: http://opg.optica.org/jlt/abstract.cfm?URI=jlt-33-19-4032

[32] J. Carpenter, B. J. Eggleton, and J. Schröder, "Observation of eisenbud–wigner–smith states as principal modes in multimode fibre," *Nature Photonics*, vol. 9, no. 11, pp. 751–757, Nov 2015.

[33] N. K. Fontaine, H. Chen, R. Ryf, D. Neilson, J. C. Alvarado, J. van Weerdenburg, R. Amezcua-Correa, C. Okonkwo, and J. Carpenter, "Programmable vector mode multiplexer," in *2017 European Conference on Optical Communication (ECOC)*, 2017, pp. 1–3.

[34] D. Pohle, S. Rothe, F. Barbosa, F. M. Ferreira, N. Koukourakis, and J. W. Czarske, "Intelligent self calibration tool for adaptive mode multiplexers using multiplane light conversion," in *25th Congress of the International Commission for Optics*. International Society for Optics and Photonics, 2022, submitted.

[35] M. Mounaix, N. K. Fontaine, D. T. Neilson, R. Ryf, H. Chen, J. C. Alvarado-Zacarias, and J. Carpenter, "Time reversed optical waves by arbitrary vector spatiotemporal field generation," *Nature Communications*, vol. 11, no. 1, p. 5813, Nov 2020.

[36] S. Pai, I. A. D. Williamson, T. W. Hughes, M. Minkov, O. Solgaard, S. Fan, and D. A. B. Miller, "Parallel programming of an arbitrary feedforward photonic network," *IEEE Journal of Selected Topics in Quantum Electronics*, vol. 26, no. 5, pp. 1–13, 2020.

[37] K. Choutagunta, I. Roberts, D. A. B. Miller, and J. M. Kahn, "Adapting mach–zehnder mesh equalizers in direct-detection mode-division-multiplexed links," *Journal of Lightwave Technology*, vol. 38, no. 4, pp. 723–735, 2020.

[38] A. Ribeiro, A. Ruocco, L. Vanacker, and W. Bogaerts, "Demonstration of a 4x4-port universal linear circuit," *Optica*, vol. 3, no. 12, pp. 1348–1357, Dec 2016.

[39] M. Kuschnerov, M. Chouayakh, K. Piyawanno, B. Spinnler, E. de Man, P. Kainzmaier, M. S. Alfiad, A. Napoli, and B. Lankl, "Data-aided versus blind single-carrier coherent receivers," *IEEE Photonics Journal*, vol. 2, no. 3, pp. 387–403, 2010.

[40] G. Milione, D. A. Nolan, and R. R. Alfano, "Determining principal modes in a multimode optical fiber using the mode dependent signal delay method," *J. Opt. Soc. Am. B*, vol. 32, no. 1, pp. 143–149, Jan 2015.

[41] I. Roudas, J. Kwapisz, and D. A. Nolan, "Optimal launch states for the measurement of principal modes in optical fibers," *Journal of Lightwave Technology*, vol. 36, no. 20, pp. 4915–4931, 2018.

[42] F. M. Ferreira, D. Fonseca, and H. J. A. da Silva, "Design of few-mode fibers with m-modes and low differential mode delay," *Journal of Lightwave Technology*, vol. 32, no. 3, pp. 353–360, 2014.

[43] J. Wuttke, P. Krummrich, and J. Rosch, "Polarization oscillations in aerial fiber caused by wind and power-line current," *IEEE Photonics Technology Letters*, vol. 15, no. 6, pp. 882–884, 2003.

[44] M. Mazur, D. Wallberg, L. Dallachiesa, E. Börjeson, R. Ryf, M. Bergroth, B. Josefsson, N. K. Fonataine, H. Chen, D. T. Nielson, J. S. P. Larsson-Edefors, and M. Karlsson, "Field trial of FPGA-based real-time sensing transceiver over 524km of live aerial fiber," in *Optical Fiber Communication Conference (OFC) 2023*. Optica Publishing Group, 2023, p. Tu3G.4.

[45] C. De Angelis, A. Galtarossa, G. Gianello, F. Matera, and M. Schiano, "Time evolution of polarization mode dispersion in long terrestrial links," *Journal of Lightwave Technology*, vol. 10, no. 5, pp. 552–555, 1992.

[46] P. Krummrich, E.-D. Schmidt, W. Weiershausen, and A. Mattheus, "Field trial results on statistics of fast polarization changes in long haul wdm transmission systems," in *OFC/NFOEC Technical Digest. Optical Fiber Communication Conference, 2005.*, vol. 4, 2005, pp. 3 pp. Vol. 4–.